NUWC-NPT Technical Memorandum 972138

Naval Undersea Warfare Center Division
Newport, Rhode Island

A BOUNDARY INTEGRAL METHOD FOR TWO-DIMENSIONAL WATER WAVES

Isaac M. Kuria
Submarine Electromagnetic Systems Department

Steven A. Trogdon
University of Minnesota

31 October 1997

Report Documentation Page

Form Approved
OMB No. 0704-0188

1. REPORT DATE	2. REPORT TYPE	3. DATES COVERED
31 OCT 1997	**Technical Memo**	**31-10-1997 to 31-10-1997**

4. TITLE AND SUBTITLE
A Boundary Integral Method for Two-Dimensional Water Waves

5a. CONTRACT NUMBER
5b. GRANT NUMBER
5c. PROGRAM ELEMENT NUMBER

6. AUTHOR(S)
Isaac Kuria; Steven Trogdon

5d. PROJECT NUMBER
5e. TASK NUMBER
5f. WORK UNIT NUMBER

7. PERFORMING ORGANIZATION NAME(S) AND ADDRESS(ES)
Naval Undersea Warfare Center Division,1176 Howell Street,Newport,RI,02841

8. PERFORMING ORGANIZATION REPORT NUMBER
TM 972138

9. SPONSORING/MONITORING AGENCY NAME(S) AND ADDRESS(ES)

10. SPONSOR/MONITOR'S ACRONYM(S)
11. SPONSOR/MONITOR'S REPORT NUMBER(S)

12. DISTRIBUTION/AVAILABILITY STATEMENT
Approved for public release; distribution unlimited

13. SUPPLEMENTARY NOTES
NUWC2015

14. ABSTRACT
A boundary integral solution to the two-dimensional, free-surface water wave problem is presented. The mathematical formulation involves application of potential theory and appropriate initial and boundary conditions to resolve the progression of the linear free-surface waves. The solution to the potential flow problem is represented, through Green's theorem, by a boundary integral method that is approximated via linear boundary panels. The resulting system of algebraic equations is solved for required flow parameters. The free surface is tracked at each time level by numerical integration of the linearized free-surface boundary conditions. Despite the use of linear panels, numerical results compare favorably with the exact linear theory and indicate that the computational scheme is able to track the development and propagation of steep waves over long periods of time. An analysis is also provided to aid in the development and numerical implementation of artificial or perfectly absorbing boundary conditions at the vertical, imaginary, truncated boundaries.

15. SUBJECT TERMS
free-surface water wave problem; free-surface waves; Green's theorem; flow parameters

16. SECURITY CLASSIFICATION OF:			17. LIMITATION OF ABSTRACT	18. NUMBER OF PAGES	19a. NAME OF RESPONSIBLE PERSON
a. REPORT	b. ABSTRACT	c. THIS PAGE			
unclassified	**unclassified**	**unclassified**	**Same as Report (SAR)**	**37**	

ABSTRACT

A boundary integral solution to the two-dimensional, free-surface water wave problem is presented. The mathematical formulation involves application of potential theory and appropriate initial and boundary conditions to resolve the progression of the linear free-surface waves. The solution to the potential flow problem is represented, through Green's theorem, by a boundary integral method that is approximated via linear boundary panels. The resulting system of algebraic equations is solved for required flow parameters. The free surface is tracked at each time level by numerical integration of the linearized free-surface boundary conditions. Despite the use of linear panels, numerical results compare favorably with the exact linear theory and indicate that the computational scheme is able to track the development and propagation of steep waves over long periods of time. An analysis is also provided to aid in the development and numerical implementation of artificial or perfectly absorbing boundary conditions at the vertical, imaginary, truncated boundaries.

ADMINISTRATIVE INFORMATION

This work was conducted under the Independent Research Program of the Naval Undersea Warfare Center (NUWC) Division, Newport, Rhode Island. The study was performed while Steven A. Trogdon of the University of Minnesota was a visiting professor at the Division in the Summer Faculty Research Program sponsored by the U.S. Navy and the American Society for Engineering Education.

TABLE OF CONTENTS

LIST OF ILLUSTRATIONS

LIST OF ILLUSTRATIONS (Cont'd)

A BOUNDARY INTEGRAL METHOD FOR TWO-DIMENSIONAL WATER WAVES

INTRODUCTION

Recent experiments by Kuria et al.,[1] as well as earlier research by other investigators,[2-9] have shown that water wave interaction can have a significant hydrodynamic effect on marine structures. Bodies of water always have surface waves, which are due to the effects of forces acting on the fluid and trying to deform it. The size and form of a surface wave will depend on the size and magnitude of the wave-generating mechanism, while its propagation will be influenced by gravity and surface tension.

The theory of water waves is provided in great detail by Dean and Dalrymple.[2] The analytical solution to the linear potential flow equations assumes that the vertical lateral boundary conditions are periodic in space and time. While it is fairly easy to implement the spatial periodic boundary condition, its quite difficult to numerically implement the temporal periodicity condition. Longuet-Higgins and Cokelet[3] used coordinate transformation to convert the computational domain to a simple closed contour. Vinje and Brevig[4] have solved the nonlinear two-dimensional wave problem in physical space. To satisfy periodic conditions at the truncated, lateral boundaries, they imposed periodicity in both velocity potential and stream function. A more general boundary integral solution to the nonlinear two-dimensional wave equation was provided by Sen et al.[5] In this work, the authors used linear panels to simulate motions of two-dimensional large floating bodies in waves.

To avoid the problems associated with lack of continuity at linear panel boundaries, Sen[6] developed a cubic-spline boundary integral method. With a cubic representation of the velocity potential in a panel, it is possible to enforce continuous velocity at the panel boundaries and corner points. Xü[7] used the boundary integral method to obtain a numerical solution to the fully nonlinear three-dimensional water wave problem in a tank. This three-dimensional boundary element method is based on biquadratic isoparametric curvilinear elements with an efficient adaptive numerical quadrature scheme. After every three or four time steps, Chebyshev smoothing was used in alternating directions to remove the three-dimensional wave instabilities.

In the research documented here, the boundary integral method is used to simulate the linear, two-dimensional wave equation in the time domain. This computational formulation is based on Green's formula for harmonic functions applied to a truncated fluid domain. To obtain a

system of algebraic equations from the Fredholm integral equations, the proposed approach applies the zeroth-order linear panels along the control boundaries. The resulting system of equations is then solved for the normal velocity and velocity potential. The tangential velocity is obtained by numerical differentiation of the velocity potential. The free surface is advanced in time by numerical integration of the linearized free-surface kinematic and dynamic boundary conditions. To start the solution, an excitation Airy wave velocity potential is imposed on the leading upstream vertical boundary. At the downstream truncation boundary, either the spatial and temporal periodicity condition or the Sommerfeld radiation boundary condition is applied.

MATHEMATICAL FORMULATION

The theory and governing physics of gravity water waves and free-surface flow are presented in Dean and Dalrymple.[2] In the physical geometry defined in figure 1, boundary ∂D_{C_2} is the location of the wave generator and ∂D_{C_1} is a fictitious boundary placed there to make the computational domain finite. Boundary ∂D_F is the free surface and ∂D_D represents a horizontal, nonporous solid boundary.

The physical coordinates (x,y) represent a point with a corresponding velocity, (u,v). The velocity components are related to the velocity potential ϕ through

$$(u,v)=\left(\frac{dx}{dt},\frac{dy}{dt}\right)=\left(\frac{\partial\phi}{\partial x},\frac{\partial\phi}{\partial y}\right). \tag{1}$$

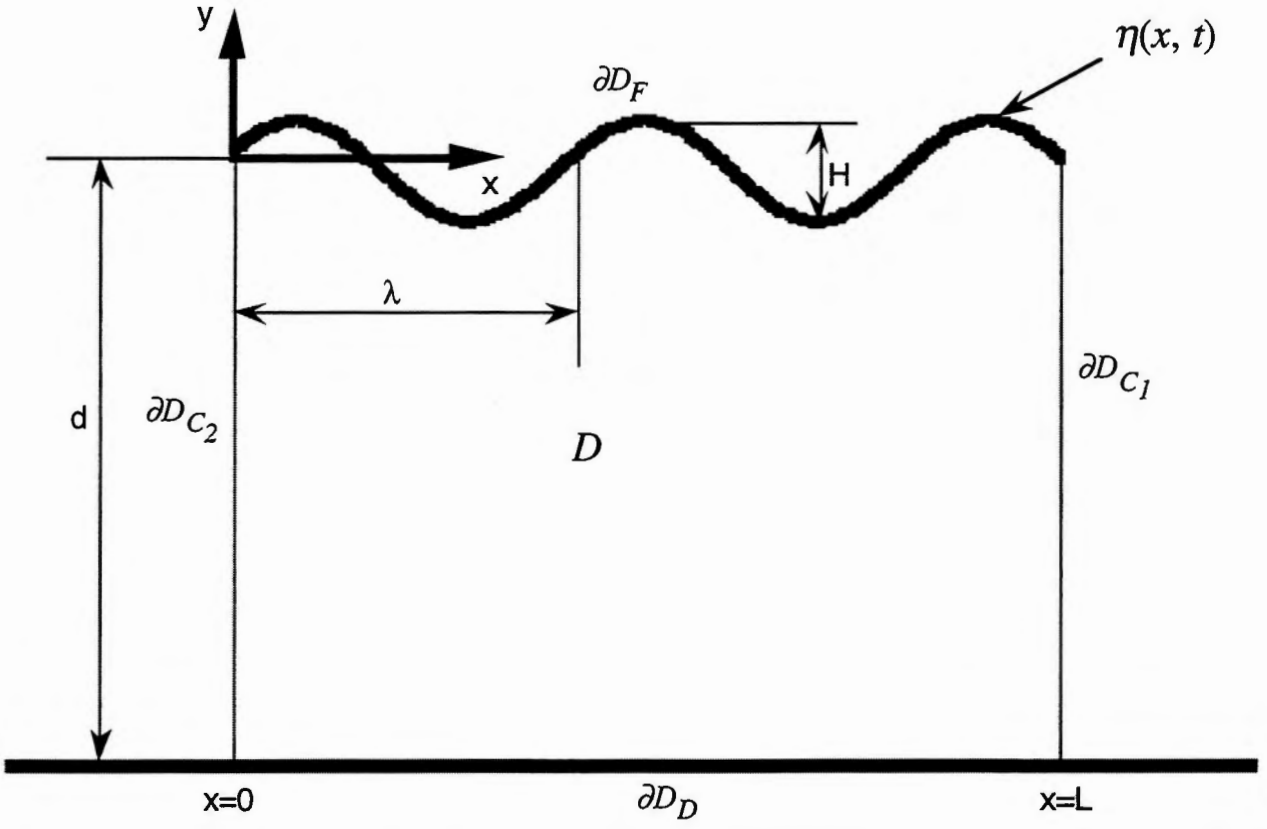

Figure 1. Geometric Definitions

We give the following definitions of the domain D and its boundary ∂D:

$$
\begin{aligned}
D &= \left\{(x,y)\,\middle|\,0<x<L\,,-d<y<\eta(x,t)\right\},\\
\partial D_F &= \left\{(x,y)\,\middle|\,0\le x\le L\,,y=\eta(x,t)\right\},\\
\partial D_{C_1} &= \left\{(x,y)\,\middle|\,x=L\,,-d\le y\le\eta(x,t)\right\},\\
\partial D_D &= \left\{(x,y)\,\middle|\,0\le x\le L\,,y=-d\right\},\\
\partial D_{C_2} &= \left\{(x,y)\,\middle|\,x=0\,,-d\le y\le\eta(x,t)\right\}.
\end{aligned}
\tag{2}
$$

With the assumption of irrotational motion and an incompressible fluid, a velocity potential exists that must satisfy the governing equation of mass conservation. In terms of the velocity potential, the continuity equation leads to the Laplace equation, which must hold throughout the fluid:

$$\nabla^2\phi = 0 \quad in \quad D. \tag{3}$$

The free-surface kinematic boundary condition requires that a fluid particle on the surface remain on the free surface. That is,

$$\frac{d}{dt}\left\{y-\eta(x,t)\right\}=0 \ \text{ on } \ y(t)=\eta(x,t)\ , \tag{4}$$

which, on expanding, gives

$$\frac{\partial\eta}{\partial t}=\frac{\partial\phi}{\partial y}-\frac{\partial\phi}{\partial x}\frac{\partial\eta}{\partial x} \ \text{ on } \ y(t)=\eta(x,t). \tag{5}$$

The pressure within the fluid domain D and on all the boundaries must conform to Bernoulli's equation. The Bernoulli equation is therefore used to obtain the dynamic free-surface boundary condition. In its irrotational form, this boundary condition is

$$\frac{\partial\phi}{\partial t}=-\frac{1}{2}\left[\left(\frac{\partial\phi}{\partial x}\right)^2+\left(\frac{\partial\phi}{\partial y}\right)^2\right]-g\eta \ \text{ on } \ y(t)=\eta(x,t). \tag{6}$$

On the rigid, nonporous bottom boundary, there can be no fluid velocity component normal to the boundary. The flow must be entirely tangential to the boundary, so that the bottom surface is always a streamline. This can be mathematically expressed as

$$\frac{\partial \phi}{\partial n} = 0 \text{ on } \partial D_D \,, \tag{7}$$

where n is the unit normal pointing outward from the computational domain.

NUMERICAL ANALYSIS

Solutions to the harmonic velocity potential may be represented by its boundary data. In a two-dimensional region, Green's second identity gives

$$\phi(\mathbf{x}) = \frac{1}{\Omega(\mathbf{x})} \int_{\partial D} \left[\phi(\xi) \frac{\partial}{\partial n} G(\mathbf{x},\xi) - G(\mathbf{x},\xi) \frac{\partial}{\partial n} \phi(\xi) \right] ds(\xi) \ , \tag{8}$$

where $\partial/\partial n$ denotes the derivative along the outward facing normal $\mathbf{n}$ on ∂D, and $G(\mathbf{x},\xi) = \ln R(\mathbf{x},\xi)$ is the kernel Green's function, where

$$R(\mathbf{x},\xi) = |\mathbf{x} - \xi| = \left[(x-\xi)^2 + (y-\eta)^2 \right]^{1/2} \tag{9}$$

is the distance between the points $\mathbf{x}$ and ξ on the boundary. The expression $\mathbf{x} = x\mathbf{i} + y\mathbf{j}$ defines any point in $\overline{D} \equiv D + \partial D$, $\xi = \xi\mathbf{i} + \eta\mathbf{j}$ defines any point on ∂D, and

$$\Omega(\mathbf{x}) = \begin{cases} \pi, & \mathbf{x} \in \text{ smooth part of } \partial D \\ \text{internal angle}, & \mathbf{x} \in \text{ corner of } \partial D \\ 2\pi, & \mathbf{x} \in D \end{cases} \ . \tag{10}$$

In boundary integral calculations, the computational domain is decomposed into many panels and an interpolation polynomial is used to approximate the velocity potential and normal velocity on each panel. The accuracy of the computational technique is improved either by an increase in the number of computational panels or by the order of the interpolation polynomial. If N is the order of the interpolation polynomial and $N_j(\xi)$ represent the cardinal functions, then the velocity potential at any point on the computational domain is approximated by

$$\phi(\xi) = \sum_{j=1}^{N} N_j(\xi) \varphi_j^s$$

and (11)

$$\frac{\partial}{\partial n} \phi(\xi) = \sum_{j=1}^{N} N_j(\xi) \psi_j^s \ ,$$

where s indicates the particular time level, i.e., $t = s(\Delta t)$ (Δt is the time step and $N_j(\xi)$ are appropriate basis functions). When linear panels are used, ϕ and $\partial\phi/\partial n$ are ultimately assumed

to be constant in each panel. In this work, it will therefore be assumed that $N_j(\xi)$ are always constant over every boundary panel. When equation (11) is substituted into equation (8), the finite dimensional approximation to $\phi(\mathbf{x})$ is found to be

$$\begin{aligned}\phi_N(\mathbf{x}) &= \frac{1}{\Omega(\mathbf{x})}\int_{\partial D}\left[\left(\sum_{j=1}^{N} N_j(\xi)\varphi_j^s\right)\frac{\partial}{\partial n}G(\mathbf{x},\xi) - G(\mathbf{x},\xi)\left(\sum_{j=1}^{N} N_j(\xi)\psi_j^s\right)\right] ds(\xi)\,, \\ &= \frac{1}{\Omega(\mathbf{x})}\sum_{j=1}^{N}\left(\int_{\partial D} N_j(\xi)\frac{\partial}{\partial n}G(\mathbf{x},\xi)\, ds(\xi)\right)\varphi_j^s - \frac{1}{\Omega(\mathbf{x})}\sum_{j=1}^{N}\left(\int_{\partial D} G(\mathbf{x},\xi)N_j(\xi)\, ds(\xi)\right)\psi_j^s\,.\end{aligned} \tag{12}$$

If we restrict $\mathbf{x} \in \partial D$ and define a projection (collocation) operator, P_N, such that

$$P_N\phi(\mathbf{x}) = \phi(\mathbf{x}_k^*)\ ,$$

the following approximation is obtained:

$$P_N\,\phi_N(\mathbf{x}) = P_N\sum_{j=1}^{N} N_j(\mathbf{x})\,\varphi_j^s = \sum_{j=1}^{N} N_j(\mathbf{x}_k^*)\,\varphi_j^s = \varphi_k^s\ , \tag{13}$$

where $\mathbf{x}_k^* \in \partial D$ are the boundary collocation points and

$$N_j(\mathbf{x}_k^*) = \delta_{jk},\quad 1 \le (j,k) \le N\,. \tag{14}$$

Applying the definition of P_N to equation (12), we obtain

$$\begin{aligned}P_N\phi_N(\mathbf{x}) = \sum_{j=1}^{N} P_N&\left(\frac{1}{\Omega(\mathbf{x})}\int_{\partial D} N_j(\xi)\frac{\partial}{\partial n}G(\mathbf{x},\xi)\, ds(\xi)\right)\varphi_j^s \\ &- \sum_{j=1}^{N} P_N\left(\frac{1}{\Omega(\mathbf{x})}\int_{\partial D} G(\mathbf{x},\xi)N_j(\xi)\, ds(\xi)\right)\psi_j^s\,.\end{aligned} \tag{15}$$

To be able to evaluate the integrals in equation (15), we partition ∂D into N panels (line segments) such that

$$\partial D = \bigcup_{i=1}^{N}\partial D_i \tag{16}$$

and

$$N_j(\xi) = \begin{cases} 1, & \xi \in \partial D_j \\ 0, & \text{otherwise.} \end{cases} \tag{17}$$

The integrals in equation (15) can therefore be written as

$$\begin{aligned} \int_{\partial D} N_j(\xi) \frac{\partial}{\partial n} G(\mathbf{x},\xi)\, ds(\xi) &= \sum_{i=1}^{N} \int_{\partial D_i} N_j(\xi) \frac{\partial}{\partial n} G(\mathbf{x},\xi)\, ds(\xi)\,, \\ &= \int_{\partial D_j} \frac{\partial}{\partial n} G(\mathbf{x},\xi)\, ds(\xi)\,, \end{aligned} \tag{18}$$

and, likewise,

$$\int_{\partial D} G(\mathbf{x},\xi) N_j(\xi)\, ds(\xi) = \int_{\partial D_j} G(\mathbf{x},\xi)\, ds(\xi)\ . \tag{19}$$

The expressions on the right-hand side of equation (15) may now be evaluated as

$$\begin{aligned} P_N\left(\frac{1}{\Omega(\mathbf{x})} \int_{\partial D} N_j(\xi) \frac{\partial}{\partial n} G(\mathbf{x},\xi)\, ds(\xi) \right) &= \frac{1}{\Omega(\mathbf{x}^*_k)} \int_{\partial D_j} \frac{\partial}{\partial n} G(\mathbf{x},\xi)\, ds(\xi) \Big|_{\mathbf{x}=\mathbf{x}^*_k} \\ &\equiv \tfrac{1}{\pi} H_{kj} \end{aligned} \tag{20}$$

and

$$\begin{aligned} P_N\left(\frac{1}{\Omega(\mathbf{x})} \int_{\partial D} G(\mathbf{x},\xi) N_j(\xi)\, ds(\xi) \right) &= \frac{1}{\Omega(\mathbf{x}^*_k)} \int_{\partial D_j} G(\mathbf{x},\xi)\, ds(\xi) \Big|_{\mathbf{x}=\mathbf{x}^*_k} \\ &\equiv \tfrac{1}{\pi} G_{kj}\,, \end{aligned} \tag{21}$$

where

$$\begin{aligned} G_{kj} &= \int_{\partial D_j} G(\mathbf{x},\xi)\, ds(\xi) \Big|_{\mathbf{x}=\mathbf{x}^*_k}\,, \\ H_{kj} &= \int_{\partial D_j} \frac{\partial}{\partial n} G(\mathbf{x},\xi)\, ds(\xi) \Big|_{\mathbf{x}=\mathbf{x}^*_k}\,, \end{aligned} \tag{22}$$

and $\Omega(\mathbf{x}_k^*) = \pi$. For our purposes, the collocation (control) points $\mathbf{x}_k^*$ will be chosen to be midpoints of ∂D_k.

Upon substituting equations (13), (20) and (21) into equation (15), the following system of equations is obtained:

$$\pi \varphi_k^s = \sum_{j=1}^{N} H_{kj} \varphi_j^s - \sum_{j=1}^{N} G_{kj} \psi_j^s, \quad 1 \le k \le N \ , \tag{23}$$

or, equivalently,

$$\pi \sum_{j=1}^{N} \delta_{kj} \varphi_j^s = \sum_{j=1}^{N} H_{kj} \varphi_j^s - \sum_{j=1}^{N} G_{kj} \psi_j^s, \quad 1 \le k \le N \ , \tag{24}$$

which may be written as

$$\sum_{j=1}^{N} \hat{H}_{kj} \varphi_j^s - \sum_{j=1}^{N} G_{kj} \psi_j^s = 0, \quad 1 \le k \le N \ , \tag{25}$$

where

$$\hat{H}_{kj} \equiv H_{kj} - \pi \delta_{kj} \ . \tag{26}$$

We next particularize the system of equations relative to two-dimensional wave generation in a rectangular cavity. The domain is given in figure 1. We partition the respective parts of ∂D as follows:

$$\begin{array}{lll} \partial D_F & 1 \le j \le npl & \phi - \text{ specified} \ , \\ \partial D_{C_1} & npl+1 \le j \le np2 & \phi - \text{ specified} \ , \\ \partial D_D & np2+1 \le j \le np3 & \dfrac{\partial \phi}{\partial n} - \text{ specified} \ , \\ \partial D_{C_2} & np3+1 \le j \le N & \phi - \text{ specified} \ , \end{array} \tag{27}$$

where $np1$, $np2 - np1$, $np3 - np2$, and $N - np3$ are, respectively, the number of boundary panels on ∂D_F, ∂D_{C_1}, ∂D_D, and ∂D_{C_2}.

Substituting the governing information given in equation (27) into equation (25), including the known boundary conditions, results in the following system of algebraic equations:

$$\sum_{j=np2+1}^{np3} \hat{H}_{kj}\varphi_j^s - \sum_{j=1}^{np2} G_{kj}\psi_j^s - \sum_{j=np3+1}^{N} G_{kj}\psi_j^s$$

$$= -\sum_{j=1}^{np2} \hat{H}_{kj}\varphi_j^s - \sum_{j=np3+1}^{N} \hat{H}_{kj}\varphi_j^s + \sum_{j=np2+1}^{np3} G_{kj}\psi_j^s , \quad 1 \le k \le N , \tag{28}$$

which may be written symbolically as

$$\mathbf{A}\mathbf{x}^s = \mathbf{b} , \tag{29}$$

where the elements of $\mathbf{x}^s$ are given by

$$\mathbf{x}^s = \begin{bmatrix} \begin{bmatrix} \psi_1^s \\ \vdots \\ \psi_{np2}^s \end{bmatrix} \\ \begin{bmatrix} \varphi_{np2+1}^s \\ \vdots \\ \varphi_{np3}^s \end{bmatrix} \\ \begin{bmatrix} \psi_{np3+1}^s \\ \vdots \\ \psi_N^s \end{bmatrix} \end{bmatrix} . \tag{30}$$

The elements of $\mathbf{A}$ are

$$\mathbf{A} = \begin{bmatrix} \begin{bmatrix} -G_{11} & \cdots & -G_{1,np2} \\ \vdots & & \vdots \\ & \ddots & \\ \vdots & & \vdots \\ -G_{N,1} & \cdots & -G_{N,np2} \end{bmatrix} & \begin{bmatrix} \hat{H}_{1,np2+1} & \cdots & \hat{H}_{1,np3} \\ \vdots & \ddots & \vdots \\ \hat{H}_{np2,np2+1} & \cdots & \hat{H}_{np2,np3} \end{bmatrix} & \begin{bmatrix} -G_{1,np3+1} & \cdots & -G_{1,N} \\ \vdots & & \vdots \\ & \ddots & \\ \vdots & & \vdots \\ -G_{N,np3+1} & \cdots & -G_{N,N} \end{bmatrix} \\ \begin{bmatrix} \hat{H}_{np2+1,np2+1} & \cdots & \hat{H}_{np2+1,np3} \\ \vdots & \ddots & \vdots \\ \hat{H}_{np3,np2+1} & \cdots & \hat{H}_{np3,np3} \end{bmatrix} & & \\ \begin{bmatrix} \hat{H}_{np3+1,np2+1} & \cdots & \hat{H}_{np3+1,np3} \\ \vdots & \ddots & \vdots \\ \hat{H}_{N,np2+1} & \cdots & \hat{H}_{N,np3} \end{bmatrix} & & \end{bmatrix}, \quad (31)$$

and the elements of $\mathbf{b}$ are

$$b_k = -\sum_{j=1}^{np2} \hat{H}_{kj}\varphi_j^s + \sum_{j=np2+1}^{np3} G_{kj}\psi_j^s - \sum_{j=np3+1}^{N} \hat{H}_{kj}\varphi_j^s, \quad 1 \le k \le N \ . \quad (32)$$

We note that the sub-block

$$\begin{bmatrix} \hat{H}_{np2+1,np2+1} & \cdots & \hat{H}_{np2+1,np3} \\ \vdots & \ddots & \vdots \\ \hat{H}_{np3,np2+1} & \cdots & \hat{H}_{np3,np3} \end{bmatrix} \quad (33)$$

is the only portion of $\mathbf{A}$ that has π subtracted along its main diagonal.

From Nachbin,[8] the matrix, as defined by equation (26), must have the following property* for any fixed $k \to i$:

$$\hat{H}_{ii} = -\sum_{\substack{j=1 \\ j\neq i}}^{N} \hat{H}_{ij} = -\sum_{\substack{j=1 \\ j\neq i}}^{N} H_{ij} = H_{ii} - \pi \ . \quad (34)$$

Therefore,

*The code we used in our simulations was modified to reflect this property.

$$H_{ii} = -\sum_{\substack{j=1 \\ j \neq i}}^{N} H_{ij} + \pi \ . \tag{35}$$

If equation (25) is to model a constant potential ϕ in each panel, then we must have $\psi_j^s = 0$, and therefore

$$\sum_{j=1}^{N} \hat{H}_{kj} \, \varphi_j^s = 0 \tag{36}$$

for any constant vector φ_j^s. Equations (34) and (35) follow immediately from equation (36). Equation (35) provides a convenient way of evaluating the second part of equation (22) when $k = j$.

In order to solve the system of algebraic equations in equation (29), expressions are required for the integrals in equation (22). To maintain legibility, the following function definitions are introduced:

$$\Psi(\mathbf{x}) = \int_{\partial D_j} \ln R \, ds(\xi) \tag{37}$$

and

$$\Phi(\mathbf{x}) = \int_{\partial D_j} \frac{\partial}{\partial n}\left(\ln R\right) ds(\xi) \ . \tag{38}$$

From figure 2, it can be seen that on ∂D_j, $\mathbf{r} = \mathbf{x} - \xi = (x - \xi)\mathbf{i} + (y - \eta)\mathbf{j}$, and therefore $R = (\mathbf{r} \cdot \mathbf{r})^{1/2} = [(x - \xi)^2 + (y - \eta)^2]^{1/2}$.

Using figure 2, we may next rewrite the integrand in equation (38) as

$$\frac{\partial}{\partial n}(\ln R) = \mathbf{n} \cdot \nabla_{\xi}(\ln R) = \frac{\mathbf{n}}{R} \cdot \nabla_{\xi} R = -\frac{\mathbf{n} \cdot \mathbf{r}}{R^2} \ . \tag{39}$$

Equation (38) thus becomes

$$\Phi(\mathbf{x}) = -\int_{\partial D_j} \frac{\mathbf{n}\cdot\mathbf{r}}{R^2} ds(\xi) \ . \tag{40}$$

Equation (22) may then be expressed in terms of equations (37) and (40) as

$$G_{kj} = \Psi(\mathbf{x}_k^*)$$

and

$$H_{kj} = \Phi(\mathbf{x}_k^*) \ . \tag{41}$$

The integrals in equations (37) and (40) are evaluated using the ideas introduced by Faltinsen.[9] The development that follows is based on the geometry of figure 2. The subscripts L and R, respectively, denote the left and right endpoints of the boundary element ∂D_j; $\mathbf{s} = \mathbf{s}(\xi)$ and $\mathbf{n} = \mathbf{n}(\xi)$, respectively, denote the unit tangent and normal to ∂D_j, where $\mathbf{s}$ points from ξ_L to ξ_R and $\mathbf{n} = \mathbf{k} \wedge \mathbf{s}$ points outward to ∂D_j at (ξ, η); and $(-s, -n)$ are the components of $\mathbf{r}$ relative to the basis $(\mathbf{s}, \mathbf{n})$. In defining the outward normal $\mathbf{n}$, it is assumed that the boundary element ∂D_j is oriented such that, relative to the direction $\mathbf{s}$, the interior of the region D is on the right (see figure 2). The following relationships are then obtained:

$$s_L \le s \le s_R \ , \tag{42a}$$

$$\mathbf{s} = \frac{\Delta\xi}{\Delta s}\mathbf{i} + \frac{\Delta\eta}{\Delta s}\mathbf{j}, \quad \mathbf{n} = -\frac{\Delta\eta}{\Delta s}\mathbf{i} + \frac{\Delta\xi}{\Delta s}\mathbf{j}, \tag{42b}$$

$$(\Delta\xi, \Delta\eta) = \big((\xi_R - \xi_L), (\eta_R - \eta_L)\big), \quad \Delta s = \sqrt{(\Delta\xi)^2 + (\Delta\eta)^2}, \tag{42c}$$

$$n = -\mathbf{n}\cdot\mathbf{r} = -\mathbf{n}\cdot\mathbf{r}_R = -\mathbf{n}\cdot\mathbf{r}_L, \quad s = -\mathbf{s}\cdot\mathbf{r} \ , \tag{42d}$$

$$\mathbf{r} = -n\mathbf{n} - s\mathbf{s}, \quad \text{and} \quad R = n^2 + s^2. \tag{42e}$$

Equation (37) therefore becomes

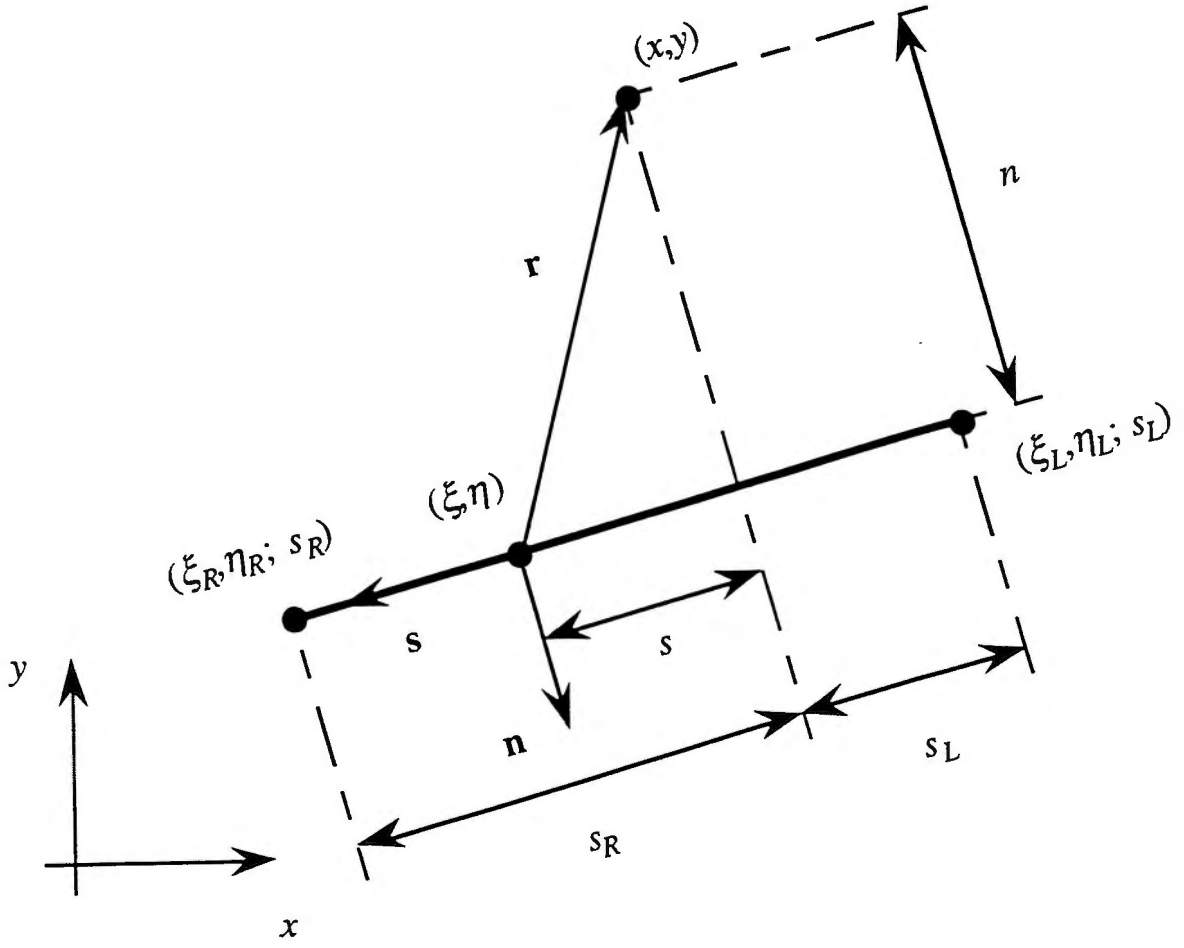

Figure 2. Geometry of the Boundary Element ∂D_j

$$\Psi(\mathbf{x}) = \int_{s_L}^{s_R} \ln R \, ds(\xi) = \int_{s_L}^{s_R} \ln\sqrt{n^2 + s^2}\, ds \,,$$

$$= \tfrac{1}{2}\left[s_R \ln\left(n^2 + {s_R}^2\right) - 2s_R + 2n\tan^{-1}\left(\frac{s_R}{n}\right) \right. \tag{43}$$

$$\left. - s_L \ln\left(n^2 + {s_L}^2\right) + 2s_L - 2n\tan^{-1}\left(\frac{s_L}{n}\right) \right] \,,$$

where $s_L = -\mathbf{s}\cdot\mathbf{r}_L$ and $s_R = -\mathbf{s}\cdot\mathbf{r}_R$. The normals may be defined either by $n = -\mathbf{n}\cdot\mathbf{r}_L$ or $n = -\mathbf{n}\cdot\mathbf{r}_R$. Similarly, equation (40) becomes

$$\Phi(\mathbf{x}) = -\int_{s_L}^{s_R} \frac{\mathbf{n}\cdot\mathbf{r}}{R^2}\, ds(\xi) = \int_{s_L}^{s_R} \frac{n}{n^2+s^2}\, ds\,,$$
$$= \left[\tan^{-1}\left(\frac{s_R}{n}\right) - \tan^{-1}\left(\frac{s_L}{n}\right)\right], \quad \mathbf{x} \notin \partial D_j\,, \tag{44}$$

where the quantities s_L, s_R, and n all depend on $\mathbf{x}$ through $\mathbf{r}_L$ and $\mathbf{r}_R$. Of particular interest is the evaluation of equation (40) when $\mathbf{x} = \mathbf{x}_j^*$, $\mathbf{x}_j^* \in \partial D_j$, and $\mathbf{x}_j^* \neq \xi_L$ or ξ_R. One obtains different values for $\Phi(\mathbf{x})_{\mathbf{x}\to\mathbf{x}_j^*}$, depending on how the limit $\mathbf{x} \to \mathbf{x}_j^*$ is taken. If the point $\mathbf{x}_j^*$ is approached through positive values of n, then for values of $\mathbf{x}$ sufficiently close to $\mathbf{x}_j^*$, it is easy to see (since $s_L < 0$ and $s_R > 0$) that

$$\lim_{\substack{\mathbf{x}\to\mathbf{x}_j^* \\ n\to 0^+}} \Phi(\mathbf{x}) = \pi\,. \tag{45}$$

If the point $\mathbf{x}_j^*$ is approached through negative values of n, then for values of $\mathbf{x}$ sufficiently close to $\mathbf{x}_j^*$,

$$\lim_{\substack{\mathbf{x}\to\mathbf{x}_j^* \\ n\to 0^-}} \Phi(\mathbf{x}) = -\pi\,. \tag{46}$$

The limit taken through positive values of n means that $\mathbf{x} \to \mathbf{x}_j^*$ from points within D, and, likewise, the limit taken through negative values of n means that $\mathbf{x} \to \mathbf{x}_j^*$ from points outside D. Finally, if the point $\mathbf{x}_j^*$ is approached through points on ∂D_j, then $n = 0$, and since s_L and s_R are independent of n, we have

$$\lim_{\substack{\mathbf{x}\to\mathbf{x}_j^*, \mathbf{x}\in\partial D_j \\ n\to 0}} \Phi(\mathbf{x}) = 0\,. \tag{47}$$

It is therefore appropriate to assume that when equation (8) is used for the potential ϕ, the latter of these three approaches is the correct way to evaluate equation (40) when $\mathbf{x} = \mathbf{x}_j^*$, $\mathbf{x}_j^* \in \partial D_j$, and $\mathbf{x}_j^* \neq \xi_L$ or ξ_R. This method of evaluating the limits is consistent with the finite dimensional approximation to the flow parameters. In these calculations, $\mathbf{x}$ has been explicitly restricted to points on ∂D. The proposed method of evaluating the limit is consistent with equation (36). When the control points are chosen to be the midpoints of ∂D_j, it can be shown that

$$\sum_{\substack{j=1 \\ j \neq i}}^{N} H_{ij} = \pi \tag{48}$$

for each fixed value of $i, 1 \leq i \leq N$. Similar results were also obtained by Nachbin[8] while using a conjugate harmonic representation for the integrand presented in equation (40). Results from boundary integral methods are known to be independent of the choice of boundary collocation points or boundary element basis.

TEST PROBLEM ALGORITHM

The accuracy of the proposed method and Green function integrals is tested with a simple problem, which is that of potential flow in a fixed, rectangular computational domain. The governing equation is the Laplace equation on a $(0,1)\times(-1,0)$ rectangular geometry with the following boundary conditions:

$$\begin{aligned}
&\phi = 2 \quad \text{on} \quad \partial D_F = \left\{(x,y) \,\middle|\, y = 0\right\}, \\
&\phi = 2 \quad \text{on} \quad \partial D_{C_1} = \left\{(x,y) \,\middle|\, x = 1\right\}, \\
&\frac{\partial \phi}{\partial y} = 0 \quad \text{on} \quad \partial D_D = \left\{(x,y) \,\middle|\, y = -1\right\}, \\
&\phi = 2 \quad \text{on} \quad \partial D_{C_2} = \left\{(x,y) \,\middle|\, x = 0\right\}.
\end{aligned} \tag{49}$$

The unique solution to this problem is the constant potential $\phi(x,y,t) = 2$. To test the applicability of the above integral equations, the problem is solved with 10 equally spaced panels on each of the four boundaries. Results are presented in figure 3 for control points located at a quarter, mid, and three quarters of the panel. As a measure of the accuracy of the numerical solution, we have graphed $\partial\phi/\partial y\big|_{y=0}$ at the collocation (control) points for different partitioning of ∂D. The exact value is $\partial\phi/\partial y\big|_{y=0} = 0, \ \forall x$, which is in excellent agreement with the values shown in figure 3, indicating that the results obtained from these integrals are independent of the location of the control points.

Another issue to be discussed is the accuracy of the numerical method when two adjacent panels are of different lengths. It should be noted that the accuracy of the linear panel numerical method is usually improved by increasing the number of panels. The question is how to arrange the same number of panels in the computational domain so that their physical geometry is adequately defined. If the physical domain is properly defined, the length of adjacent panels will have negligible effect on the results. In figure 4, the Chebyshev-Gauss-Lobatto points were used to define the physical geometry. These points are known to produce a grid that is coarse at the end points and sparse at the middle. The control points were placed at the middle of each panel in each case presented. Figure 4 shows that despite the fact that the panels were of different lengths, the results completely agree with those for the equally spaced panels of figure 3. This indicates that the length of adjacent panels does not significantly affect the accuracy of the computational domain.

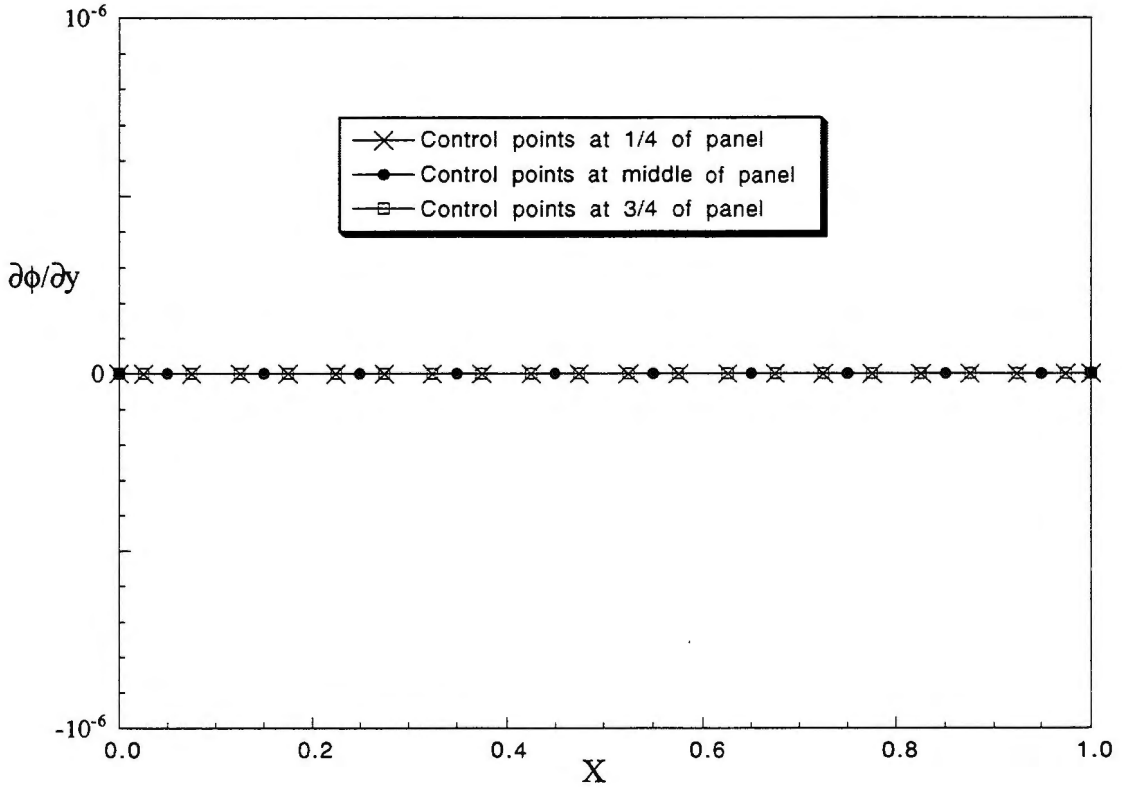

Figure 3. Computed Values of $\partial\phi/\partial y$ with Different Control Points $\left(np1 = np2 = np3 = np4 = 10;\ N = 40\right)$

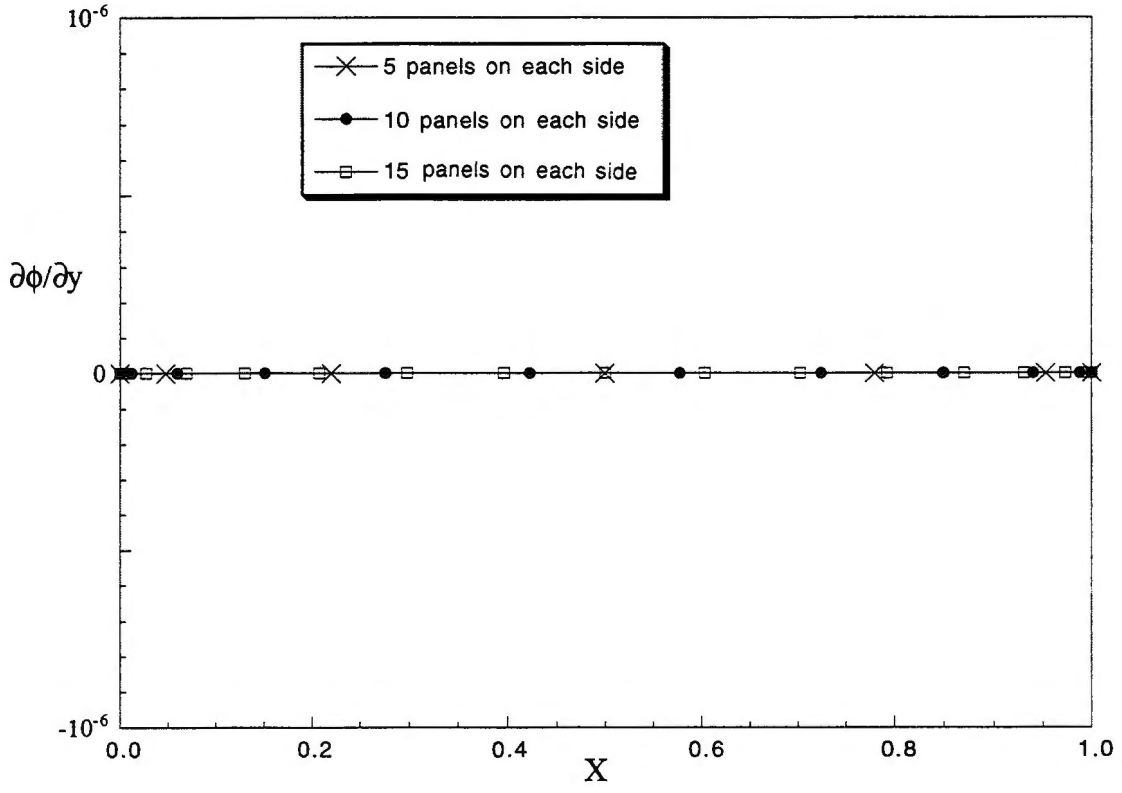

Figure 4. Computed Values of $\partial\phi/\partial y$ with Different Panel Lengths

NUMERICAL RESULTS

Next we consider the numerical solution to the linearized water wave problem as defined by the Fredholm integral relation presented in equation (8). To simulate the propagation of an Airy wave in the computational domain, the initial value of the velocity potential on the undisturbed free surface, obtained from the periodic linear solution, is

$$\phi(t) = \frac{H\lambda}{2T}\frac{\cosh(k(y+d))}{\sinh(kd)}\sin(kx-\sigma t) \ . \tag{50}$$

This velocity potential excitation is chosen to correspond to an Airy wave of height H, wavelength λ, and period T propagating in the positive x-direction. Other parameters are $k = 2\pi/\lambda$, which represents the wavenumber, and $\sigma = 2\pi/T$, which is the wave frequency.

To complete specifications of the boundary value problem, conditions must also be specified on the remaining lateral boundaries, ∂D_{C_2} and ∂D_{C_1}. For the initial linear solution, the Airy wave excitation described by equation (50) is applied on the upstream vertical boundary, and spatial and temporal periodicity is maintained on the downstream boundary. For the wave excitation described by equation (50), periodicity is achieved by applying the same potential downstream.

Numerically, the free-surface profile and velocity potential must be recovered after every period. The governing equation and boundary conditions are to be evaluated using the boundary integral methods presented in this memorandum. To advance the solution in time, the fourth-order Adams-Bashforth (AB4) method was used. The fourth-order Runge-Kutta (RK4) method was also tested and compared to AB4; both methods were shown to give the same results. Since AB4 only needs calculations from previous time levels and, unlike RK4, does not require solving Laplace's equation four times at every time-level, AB4 was found to be more computationally efficient and was thus used for the numerical calculations presented in this section. To start the solution, the lower order Adams-Bashforth method was used with correction until there was enough information to use AB4 without correcting.

In water wave theory, the free-surface boundary conditions must be satisfied on the free surface $y = \eta(x,t)$, which is *a priori* unknown. A convenient method for evaluating these conditions is to expand them at $y = 0$ (a known location) by the truncated Taylor series. The dynamic free-surface boundary condition, equation (6), therefore becomes

$$\left(\frac{\partial\phi}{\partial t}+\frac{1}{2}(\nabla\phi)^2+gy\right)_{y=\eta}=\left(\frac{\partial\phi}{\partial t}+\frac{1}{2}(\nabla\phi)^2+gy\right)_{y=0}$$

$$+\eta\frac{\partial}{\partial y}\left(\frac{\partial\phi}{\partial t}+\frac{1}{2}(\nabla\phi)^2+gy\right)_{y=0}+\cdots\cdots\cdots=0, \tag{51}$$

where the pressure is taken to be ambient on the free surface. Retaining the terms that are linear in the small parameter η, and recalling that η is only a function of x and t, the linearized dynamic free-surface boundary condition becomes

$$\left(\frac{\partial\phi}{\partial t}+g\eta\right)_{y=0}=0\ . \tag{52}$$

The kinetic free-surface boundary condition is similarly linearized to become

$$\frac{\partial\eta}{\partial t}=\left.\frac{\partial\phi}{\partial y}\right|_{y=0}\ . \tag{53}$$

Since the linearized equations are applied on the undisturbed free surface $y = 0$, the entire computational boundary is independent of time. Consequently, the influence coefficients in the resulting system of linear equations remain unchanged in time.

Computed free-surface progressions with time for a wave with an amplitude of 0.4 m, wavelength of 2.46 m (steepness of 0.33), depth of 4.0 m, and overall axial length of 4 wavelengths are presented in figure 5. A time step, Δt of 0.001 s, was used in these simulations. The other parameters, such as wave frequency and period, were obtained from the linear water wave theory. The results show that the proposed method can obtain wave propagation over a long period of time.

Figure 6 shows results for free-surface progressions near the upstream boundary at x = 0.44 m, near the center at x = 4.87 m, and near the downstream boundary at x = 9.4 m. Even near the boundaries, it is seen that the computed results compare favorably with the exact linear solution.

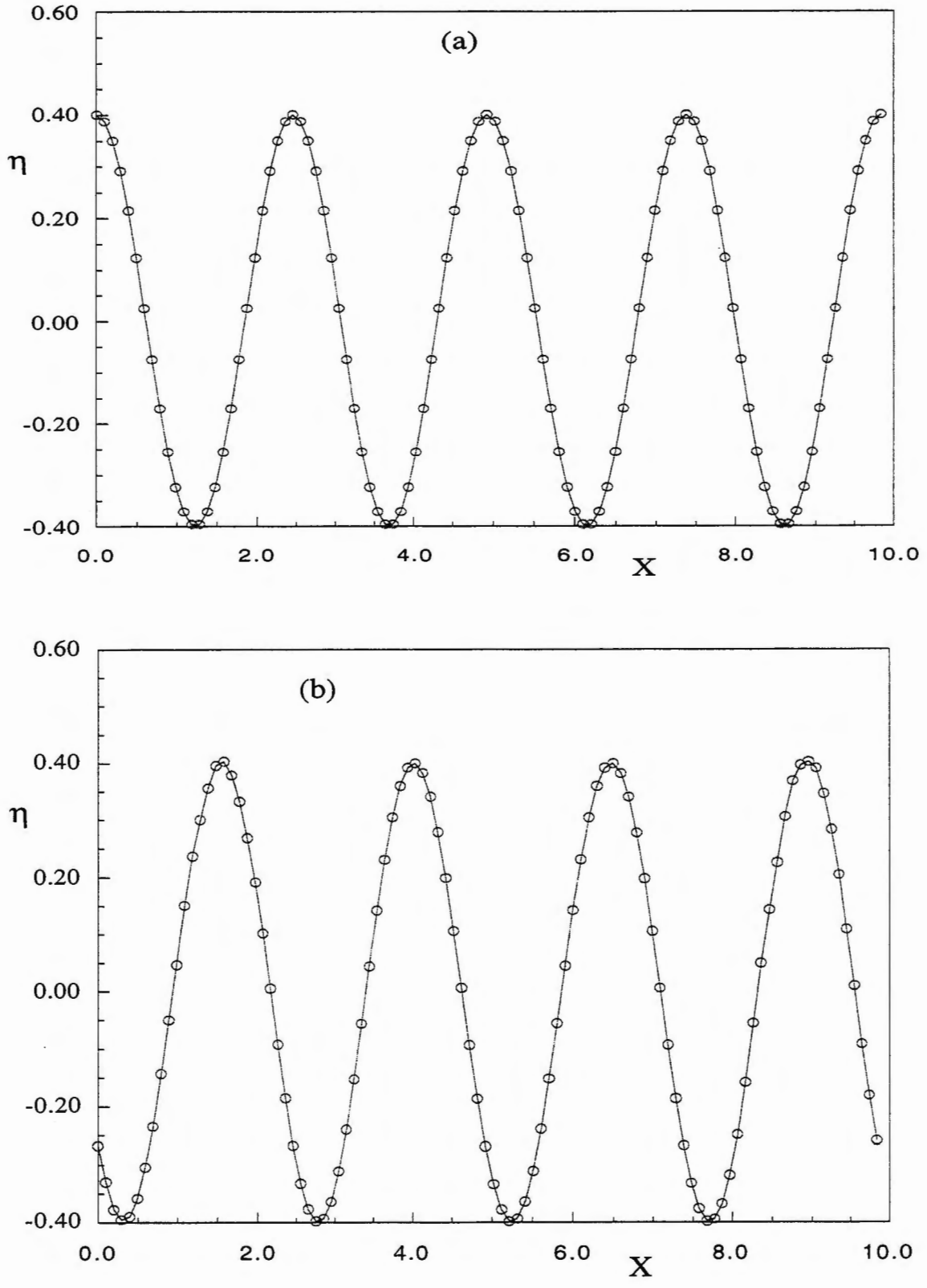

Figure 5. Free-Surface Elevations at (a) Time = 0 and (b) Time = 3.3 s

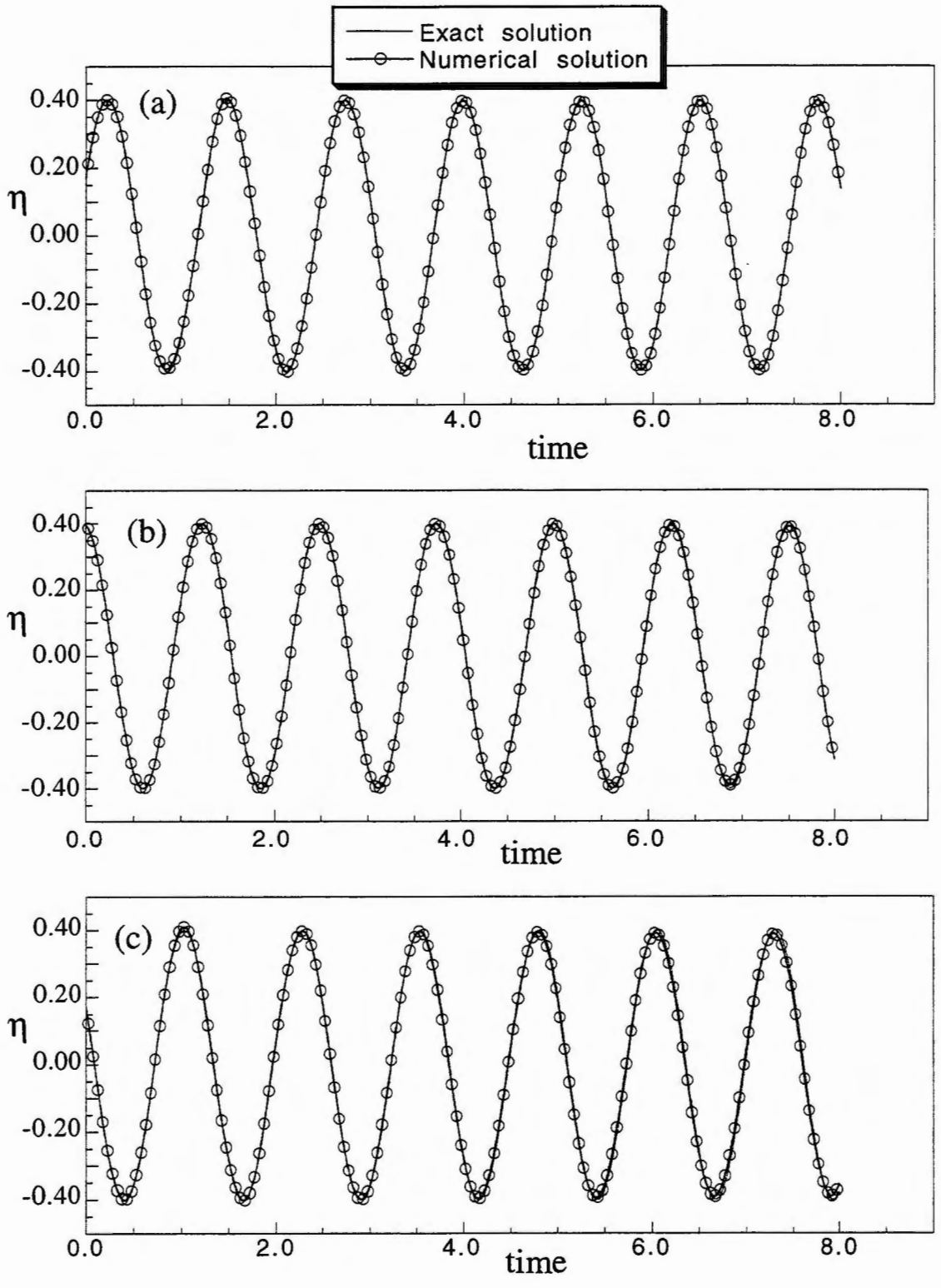

Figure 6. Free-Surface Elevations at (a) x = 0.44 m, (b) x = 4.87 m, and (c) x = 9.4 m from the Upstream Boundary

The challenge of the water wave problem is to be able to simulate the fully nonlinear wave. The linear study presented in this memorandum involves the first phase of development, which is focused on determining the appropriate boundary conditions. Though the free-surface boundary conditions are well known, the free surface itself is not defined. Another boundary problem concerns the truncated upstream and downstream boundaries. Though these boundaries are known, their boundary conditions still remain a major area of research. The actual problem is, in fact, due to these boundaries being artificial rather than real; they are there only to truncate the computational domain.

In this work, the upstream boundary (*at* $x = 0$) is simulated by a piston wavemaker. A velocity potential is therefore applied to this boundary at all times. Although another alternative would be to impose the wavemaker velocity on this boundary, the velocity potential alternative is preferred here because application of the normal velocity would require a moving upstream boundary. A stationary upstream boundary allows one to use a fully Eulerian computational scheme.

For the results presented in figures 5 and 6, the linear theory was used to obtain the downstream boundary condition. While this works well for linear waves, convergence problems would be expected with nonlinear waves. To achieve a more open downstream boundary condition, the Sommerfeld radiation condition is proposed. The radiation condition is derived from the wave equation

$$\frac{\partial^2 \phi}{\partial t^2} = C^2 \frac{\partial^2 \phi}{\partial x^2} \ , \tag{54}$$

where ϕ is any quantity and C is the phase velocity of the waves. The above equation can be written as

$$\left(\frac{\partial}{\partial t} + C \frac{\partial}{\partial x} \right) \left(\frac{\partial}{\partial t} - C \frac{\partial}{\partial x} \right) \phi = 0 \ . \tag{55}$$

The first term on the left-hand side of equation (55) represents a wave traveling in the positive x-direction with a speed of C. For this wave, the above equation is solved to give the radiation downstream boundary condition as follows:

$$\frac{\partial \phi}{\partial t} = -C \frac{\partial \phi}{\partial x} \quad . \tag{56}$$

Based on the same parameters as those of figure 5, the downstream results from this boundary condition, as presented in figure 7, compare favorably to the free-surface progressions of figure 5.

The radiation boundary condition has been tested with waves of different depth and steepness. Results for the wave elevation at fixed axial coordinates with a steepness of 0.33 are presented in figure 8. In figure 9, analytical and computed results for a wave with a depth of 2.01 m and with a steepness of 0.08 are also in good agreement.

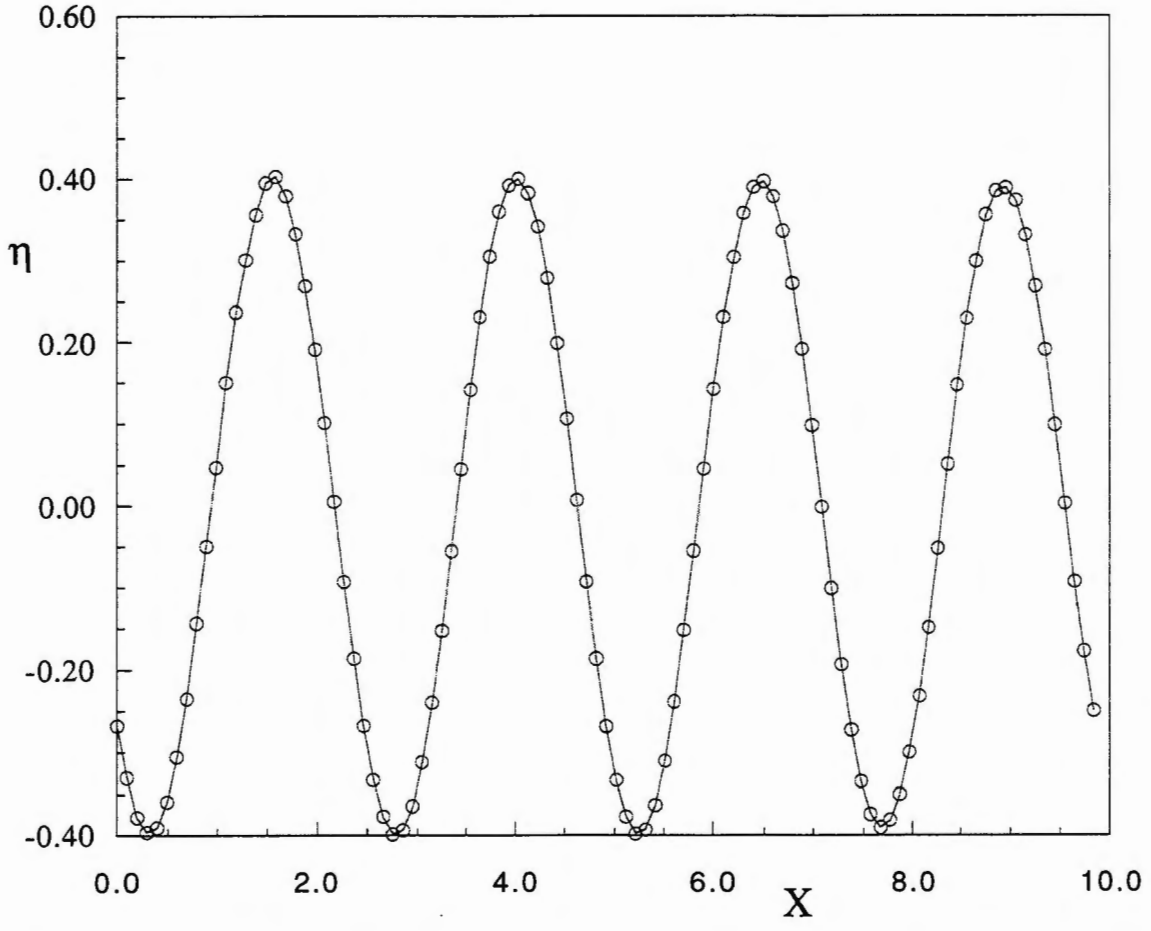

Figure 7. Free-Surface Elevations at Time = 3.3 s with the Sommerfeld Radiation Condition Used at the Downstream Boundary

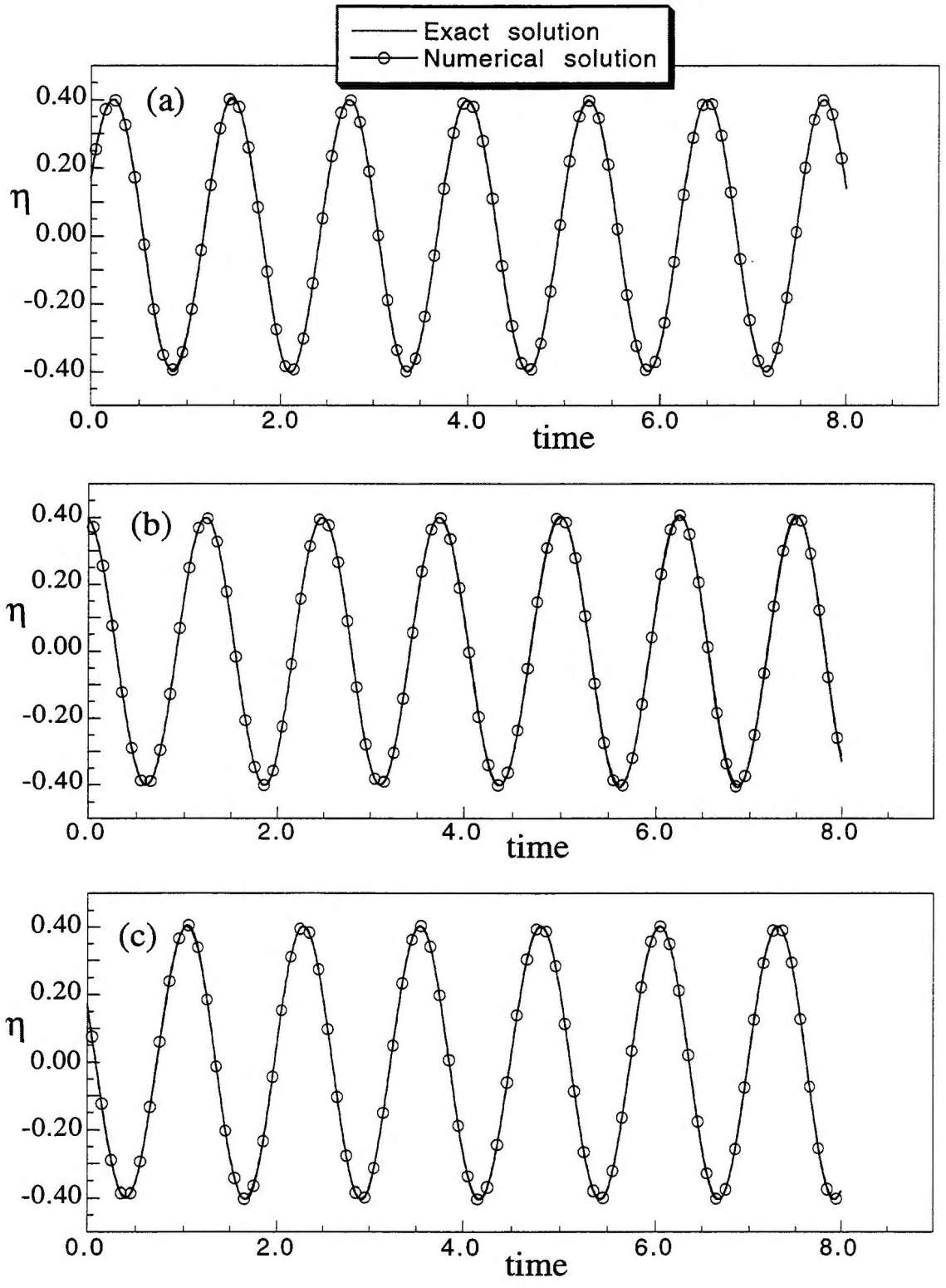

Figure 8. Free-Surface Elevations for a Steepness of 0.33 at (a) x = 0.44 m, (b) x = 4.87 m, and (c) x = 9.4 m from the Upstream Boundary with the Sommerfeld Radiation Condition Used at the Downstream Boundary

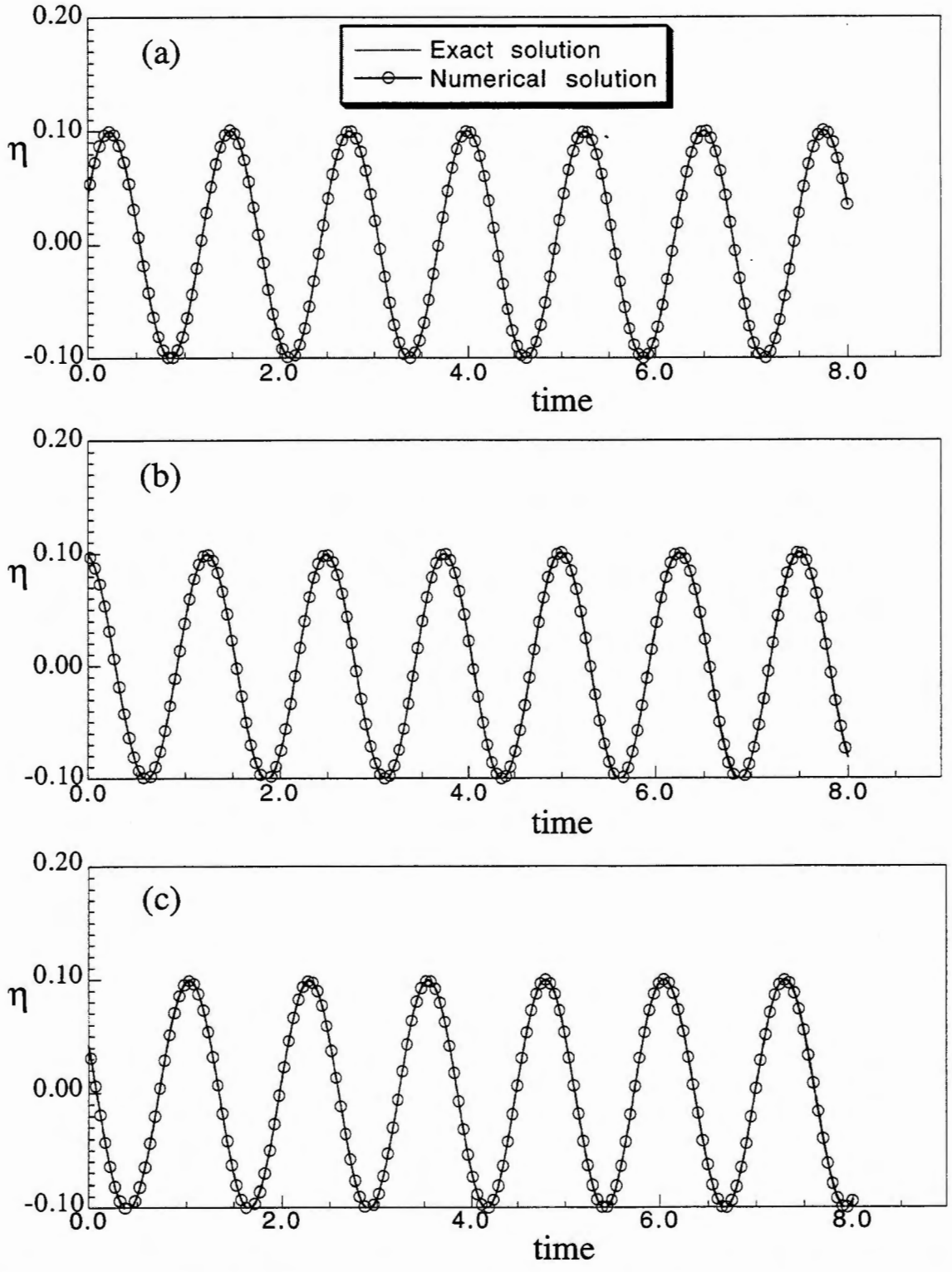

Figure 9. Free-Surface Elevations for a Steepness of 0.08 at (a) x = 0.44 m, (b) x = 4.87 m, and (c) x = 9.4 m from the Upstream Boundary with the Sommerfeld Radiation Condition Used at the Downstream Boundary

In figure 10, the wave was started with the fluid at rest $\left(\phi = \eta = 0 \text{ on } y = \eta(x,t)\right)$. A wavemaker, programmed as in equation (50) to produce an Airy wave, is placed at the upstream boundary, and the wave is allowed to propagate freely downstream. The free surface, initially at rest, is only developed by the wavemaker. The downstream boundary is four wavelengths from the upstream boundary. The water depth is 4 m and the applied upstream Airy wave velocity potential has a steepness of 0.33. These are the same parameters as were used in figures 5 and 7. The results show that once the wave is developed from the fluid at rest, the boundary integral method is able to simulate the wave over a long period of time.

In figure 10, the wavemaker was positioned upstream throughout the computational period. To avoid a velocity potential jump at the upstream/free-surface interface at the beginning of the experiment, the wavemaker was started from zero. As can be seen, it took the wavemaker one wave period to reach the steady operating condition as defined by the Airy wave. With time, the wave excitation on the left boundary produces a wave with a steepness of about 0.33 and a period of 1.26 s. These are the same free-surface wave properties obtained from linear theory.

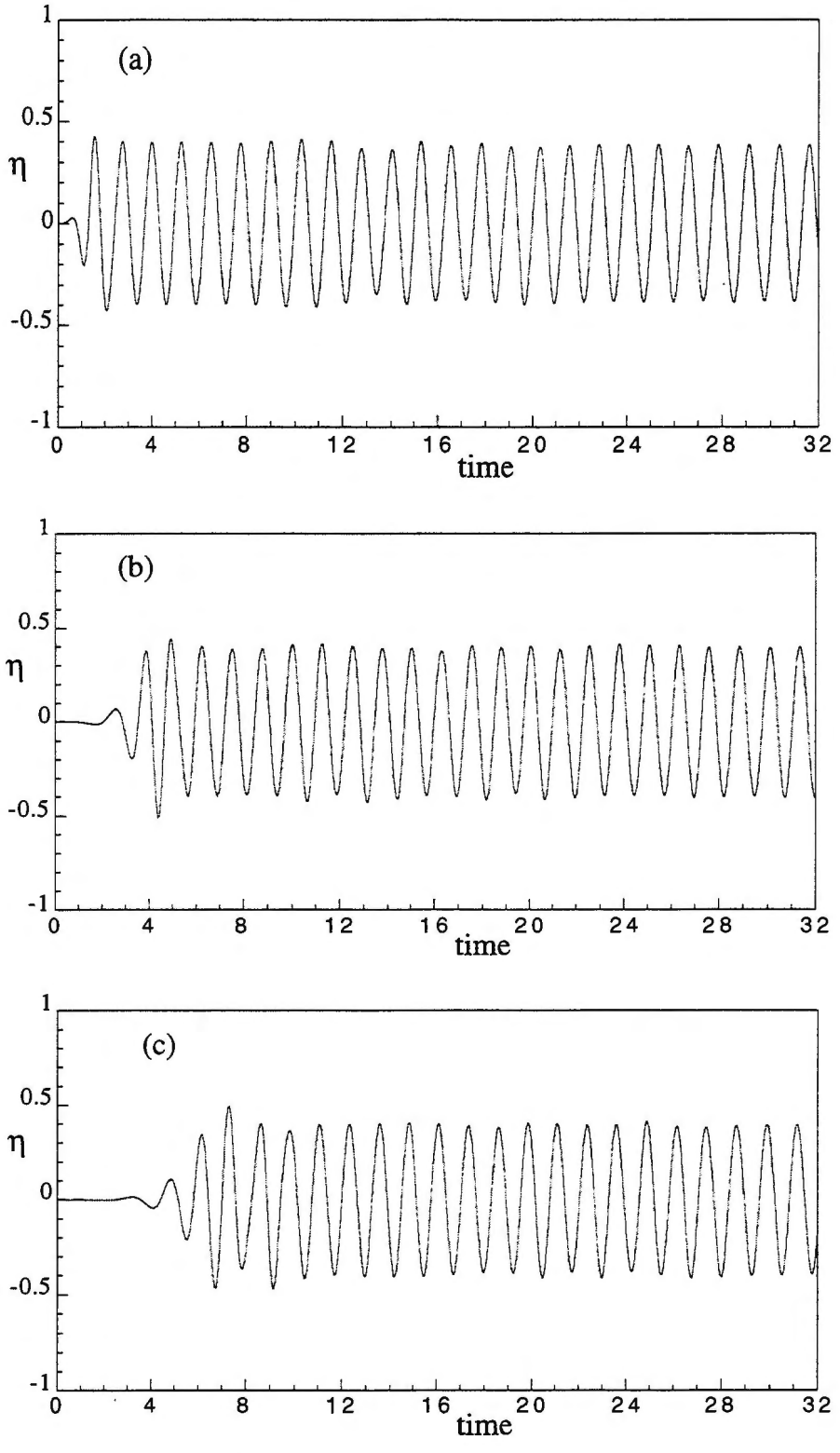

Figure 10. Free-Surface Elevations for a Wave Started from Rest at (a) x = 0.44 m, (b) x = 4.87 m, and (c) x = 9.4 m from the Upstream Boundary with the Sommerfeld Radiation Condition Used at the Downstream Boundary

CONCLUSIONS

A numerical method for simulating the propagation of steep, transient, linear, free-surface water waves has been presented. The method is based on boundary integral relations utilizing linear panels, with time marching performed via the fourth-order Adams-Bashforth algorithm. This algorithm is preferred because at every time level only one solution to the Laplace equation is required. To obtain starting values, a predictor-corrector method was used during the first three time levels. The results demonstrate that even with the linear panels and the fluid started from rest, the numerical method is capable of tracking the progression of steep, free-surface waves. Also observed is a close agreement of these results with the analytical linear solution.

It is important to note that the proposed method does not depend on water depth or on wave properties such as speed or wavelength. This capability for tracking waves generated from rest without restrictions on wave properties will be essential in extending the method to the fully nonlinear water wave problem.

REFERENCES

1. I. M. Kuria, J. H. Duncan, D. Coder, H. Parkhust, D. L. Kriebel, and J. J. Zseleczky, "Impact of Plunging, Breaking Waves on Towed Antenna Masts," NUWC-NPT Technical Memorandum 972116, Naval Undersea Warfare Center Division, Newport, RI, 1997.

2. R. G. Dean and R. A. Dalrymple, *Water Wave Mechanics for Engineers and Scientists,* Prentice Hall, Inc., Engelwood Cliffs, NJ, 1984.

3. M. S. Longuet-Higgins and E. D. Cokelet, "The Deformation of Steep Surface Waves on Water. I: A Numerical Method of Computation," *Proceedings of the Royal Society of London A*, vol. 350, 1976, pp. 1-26.

4. T. Vinje and P. Brevig, "Numerical Simulation of Breaking Waves," *Advances in Water Resources,* vol. 4, 1981, pp. 77-82.

5. D. Sen, J. S. Pawlowski, J. Lever, and M. J. Hinchey, "Two-Dimensional Numerical Modelling of Large Motions of Floating Bodies in Waves," *Proceedings of the 5th International Conference on Numerical Ship Hydrodynamics*, 1989, pp. 257-277.

6. D. Sen, "Numerical Simulation of Motions of Two-Dimensional Floating Bodies," *Journal of Ship Research*, vol. 37, no. 4, 1993, pp. 307-330.

7. H. Xü, "Numerical Study of Fully Nonlinear Water Waves in Three Dimensions," Ph.D. Thesis, Massachusetts Institute of Technology, Cambridge, MA, 1992.

8. A. Nachbin, *Modelling of Water Waves in Shallow Channels*, Computational Mechanics Publications, Boston, MA, 1993.

9. O. M. Faltinsen, "A Numerical Nonlinear Method of Sloshing in Tanks with Two-Dimensional Flow," *Journal of Ship Research*, vol. 22, no. 3, 1978, pp. 193-202.

BIBLOGRAPHY

Anderson, J. D., *Fundamentals of Aerodynamics*, McGraw-Hill Book Co., NY, 1984.

Chow, C-Y., *An Introduction to Computational Fluid Mechanics*, John Wiley & Sons, Inc., NY, 1979.

Engquist, B., and Majda, A., "Absorbing Boundary Conditions for the Numerical Simulation of Waves," *Mathematics of Computation,* vol. 31, no. 139, 1977, pp. 629-651.

Israeli, M., and Orszag, S. A., "Approximation of Radiation Boundary Conditions," *Journal of Computational Physics*, vol. 41, 1981, pp. 115-135.

Lamb, H., *Hydrodynamics*, 6th ed., Dover Publications, Mineola, NY, 1945.

Orlanski, I., "A Simple Boundary Condition for Unbounded Hyperbolic Flows," *Journal of Computational Physics*, vol. 21, 1976, pp. 251-269.

Sen, D., "Interaction of Steep Waves with Vertical Walls," *Journal of Waterways, Port, Coastal, and Ocean Engineering,* vol. 115, no. 5, American Society of Civil Engineers, 1992, pp. 453–473.

Taylor, M. E., "Reflection of Singularities of Solutions to Systems of Differential Equations," *Communications in Pure and Applied Mathematics,* vol. 28, 1975, pp. 457-478.

DISTRIBUTION LIST

External
University of Minnesota, Duluth, MN (S. A. Trogdon) (2)
American Society for Engineering Education, Washington, DC

Internal
Codes: 10
102 (S. Dickinson) (2)
30
30A
34
341
342
343
3433 (T. Floyd, I. Kuria (3))
3493 (C. McMillan)
3496 (F. Allard)
5431 (K. Holt)
70
5441 (2)
81
811
812
821
823

Total: 27